Capture of negative muons in cubic and hexagonal structures of carbon and boron nitride

H. Schneuwly, M. Boschung, K. Kaeser, G. Piller, A. Rüetschi, L. A. Schaller, and L. Schellenberg
Institut de Physique de l'Université, CH-1700 Fribourg, Switzerland
(Received 12 July 1982)

Muonic x-ray intensities of the Lyman series have been measured in carbon (diamond, graphite, and soot) and in boron and nitrogen in the cubic (diamond) and hexagonal (graphite) structures of boron nitride. By means of muon cascade calculations which reproduce the measured intensities, angular momentum distributions of the captured muons have been determined for carbon and nitrogen in the μ-atomic level $n=13$. The boron-to-nitrogen capture ratios have been found to be 0.233 ± 0.011 in the cubic structure and 0.275 ± 0.012 in the hexagonal structure. The difference of $18\pm3\%$ has to be attributed to the difference in the solid-state structures.

I. INTRODUCTION

Negative muons bound in atoms have been used for years as a tool in studies of nuclear properties like charge radii, quadrupole moments, magnetic hyperfine constants, etc. The positive muons have found a wide field of applications, e.g., in solid-state physics where inner magnetic fields are measured by the muon spin rotation (μSR) method. There is some hope that negative muons could also be used as a probe to test the distributions of bonding electrons in solids, liquids, and gases through the formation and deexcitation mechanisms of muonic atoms. Correlations of pion capture rates in hydrogen of hydrogen containing substances with various chemical parameters have already been obseved (see, e.g., Ref. 1). However, in spite of the numerous muonic capture ratios and cascade intensities measured in compounds of other elements, there is still a lack of precise data. Such data should provide information about the manner in which the electron distributions govern the formation mechanism of muonic atoms.

The aim of the present investigation was to determine a relation between the muonic x-ray intensities and the spatial structures of two comparable allotropes of carbon and boron nitride. Furthermore, the results of this experiment should enable us to test which hypotheses about the muonic capture mechanism can be retained and which ones should be rejected. In particular, we sought to determine whether there exists a correlation between the x-ray intensity patterns and the capture ratios. Our model for the Coulomb capture of muons actually contains such a correlation as a consequence of its basic hypotheses.[1,2]

To attain our aim we have measured the x-ray intensities of the Lyman series in the hexagonal and cubic structures of carbon and of boron nitride. From the measured intensities we deduced distributions over angular momentum states for the captured muons using cascade calculations. We determined the boron-to-nitrogen capture ratios in the two allotropes in order to check whether differences in the solid-state structures give a measurable difference in this ratio.

Both carbon and boron nitride have diamond and graphitic allotropies or, equivalently, cubic and hexagonal structures. Moreover, they are isoelectronic solids. As a result of these great similarities one expects, if the electron density distributions govern the muon capture mechanism, to find similarities between the muonic carbon and the muonic boron-nitride x-ray intensity patterns, or at least in the differences between the allotropes. In low-Z elements like those chosen here, the muon capture should be particularly sensitive to the electronic structure.[3] In order to check the consistency of possible interpretations we have also measured the muonic x-ray intensities in soot. The latter ones must be compared to those of graphitic carbon, the only difference in the structures of the target materials being the sizes of the crystallites.

The muonic x rays in carbon and boron nitride in both solid-state structures have already been measured in an earlier experiment.[4] However, the experimental uncertainties were too large to draw definite conclusions about differences or similarities although the trends were the same as observed in this work.

II. EXPERIMENT

The measurements were performed at the superconducting muon channel μE2 of the Swiss Institute for Nuclear Research (SIN) at Villigen. The experimental setup, the data collection system, and the

procedures for data analysis were similar to earlier experiments.[5-7]

The stopped muons were identified with a conventional telescope consisting of four scintillation counters of suitably chosen areas. The targets were placed between the last two counters at 45° with respect to the muon beam axis. In order to obtain a maximum stop rate in the relatively thin targets (1 g/cm^2 in the beam direction), 8.5 cm of beryllium were placed in front of the third scintillation counter to slow down the incoming muons of 120-MeV/c momentum. About 12% of the 10^6 sec^{-1} incoming muons gave a muon stop signal.

The muonic x rays were registered with two Ge detectors, a 2-cm^3 one placed at 90° and an intrinsic 13-cm^3 one placed at 60° with respect to the muon beam axis. The in-beam energy resolutions [full width at half maximum (FWHM)] for the muonic $2p$-$1s$ carbon line at 75 keV were 570 eV for the smaller detector and 960 eV for the larger one at counting rates of the order of 5 kHz. The smaller detector was placed at 10 cm from the target center and the larger one at 23 cm. The events registered by the Ge detectors were analyzed by 8000-channel analog-to-digital converters (ADC's). The energy range extended to 300 keV (37 eV per channel) for the smaller detector and to 400 keV (50 eV per channel) for the larger one. In order that only target events were registered in the detectors, cylindrical collimators were employed. They prevented radiation resulting from muon capture in the scintillation counters of the telescope to reach the detectors.

Prompt and delayed events with respect to the muon stop signal were registered and stored in separate spectra. For the prompt events a time window of 40 nsec was used starting with the muon stop signal. The delayed events were those recorded within a time interval from 40 to 160 nsec after a muon stop. The separation of prompt and delayed events permitted us to determine whether or not the muonic x-ray lines of interest were sitting on a background of nuclear gamma rays resulting from nuclear muon capture in the target or the shielding.

The intensity calibration has been performed off- and on-line using ^{133}Ba, ^{182}Ta (Ref. 8), ^{57}Co, ^{109}Cd, and ^{241}Am (Ref. 9) sources to cover the energy region of interest. For the off-line intensity calibration, the sources were placed in the position of the target. For the on-line intensity calibration, they were placed in such a way as to be seen by the detectors without being covered by the target. The on-line calibration events were defined as events in coincidence with an incoming muon which gave no stop signal in order to have the same time structure for the calibration events as for the muonic events. The time window for the calibration events was 200 nsec long. The stronger calibration lines due to accidental coincidence were recorded in the delayed and prompt spectra. A detailed comparison of the intensity calibrations obtained from the different on-line spectra as well as from the off-line calibration spectra was performed in order to check the influence of different electronic conditions.[10] The analysis showed under which conditions off-line intensity calibrations could be used for the prompt spectra, i.e., for the intensity determination of the muonic x rays. The γ-ray intensity sources have also been used for the energy calibration of the muonic x rays. From the precisely determined energies of the muonic np-$1s$ transition nuclear charge radii have been calculated for beryllium, boron, carbon, and nitrogen and published in a separate paper.[7]

Three carbon, two boron nitride and an aluminum target, the last one serving for background checks, have been measured successively in the same running period. The target materials were contained between a 0.038-g/cm^2 thick disk of beryllium of 7.4-cm diam and a thin foil of aluminum (0.001 g/cm^2), within a 0.3-cm thick ring of beryllium. The thicknesses of all targets were chosen to be 1 g/cm^2 in the beam direction. To obtain an additional check on the boron-to-nitrogen capture ratios, the two boron-nitride targets were remeasured several months later using a 66-cm^3 high-purity Ge detector with an in-beam resolution of 780 eV for the muonic $2p$-$1s$ carbon line at 75 keV.

The carbon-diamond target consisted of small crystallites of synthetic diamond of less than 60-μm average diameter. The carbon-graphite target had standard particle sizes of the order of 30 μm corresponding to a specific surface area of 0.1 m^2/g (Lonza graphite KS 75). The soot was composed of crystallites with diameters of the order of 30 nm corresponding to a specific surface area of the order of 100 m^2/g (Degussa printex 3).

III. ANALYSIS AND RESULTS

Figure 1 show part of the prompt spectrum of boron nitride (diamond structure) measured with the 2-cm^3 Ge (Li) detector. The intensities of the muonic x-ray peaks were extracted from the measured spectra with the use of the LINFIT computer code described in earlier papers.[5,6] The fitting procedure was applied to the sum of prompt plus delayed spectra. The correction for the absorption in the targets was calculated employing the tables given by Storm and Israel.[11] The correction varied only by 1% in the energy range between 50 and 130 keV. The uncertainty in this correction is therefore negligible with regard to the uncertainty in the detector effi-

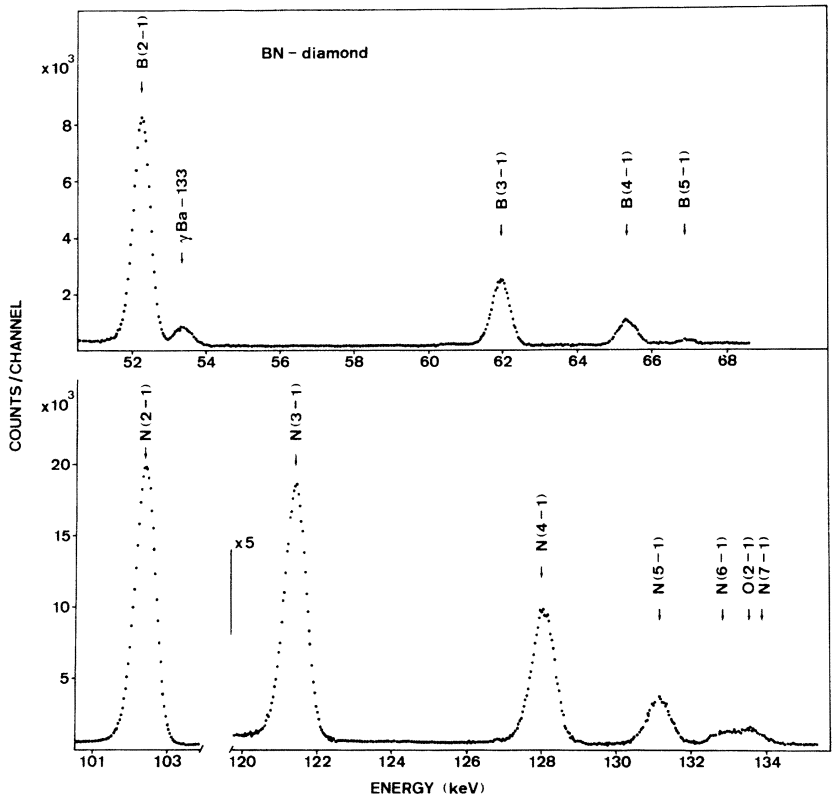

FIG. 1. Portion of the prompt spectrum of muonic boron nitride in diamond structure measured with the 2-cm^3 Ge(Li) detector. Energy resolution for the boron (2-1) transition was 530 eV at 52 keV and for the nitrogen (2-1) transition 600 eV at 102 keV. At 53 keV there is a ^{133}Ba γ line from an efficiency calibration source which was fed into the prompt spectrum by accidental coincidence.

ciency.

Table I gives the measured muonic x-ray intensities of the Lyman series in the three carbon targets relative to the $2p$-$1s$ intensity. The errors in the intensity of the strong lines are mainly due to the uncertainty in the relative efficiency calibration of the detectors whereas those of the low-intensity higher-energy transitions come from the uncertainty in the determination of the background. The relative intensities measured with the two detectors are in good agreement with each other showing that no significant systematic error occurred. In addition, it shows that measuring at 90° or 60° relative to the muon beam axis gives no detectable difference in the relative intensities.

In the three carbon targets, all relative intensities, with the exception of the (6-1):(2-1) ratio, are different. Knight *et al.*[4] obtained relative intensities which are similar with ours. However, due to their larger errors they had to conclude that the intensity patterns were essentially the same in the diamond and in the graphitic forms of carbon. Relative to graphite, corresponding intensities are systematically lower in diamond and systematically higher in soot in our measurements. This behavior is illustrated in Fig. 2 where the ratios of relative intensities are plotted. In these ratios the uncertainties in the efficiency calibration cancel so that essentially only the statistical errors remain.

The measured muonic x-ray intensities of the Lyman series in the two boron-nitride targets are listed in Table II for boron and nitrogen relative to the respective $2p$-$1s$ intensities. The data taken with the two detectors are consistent with each other and with most of the relative intensities given by Knight *et al.*[4] The (6-1) line in nitrogen causes some problems not only because of the uncertainty in the continuous background but also due to the proximity of the oxygen (2-1)-background line.

In the hexagonal modification of boron nitride all relative muonic intensities of nitrogen are larger than the corresponding intensities in the diamond modification. This is not the case for the muonic boron intensities. The comparison of the relative muonic intensities between the graphitic and the dia-

TABLE I. Relative muonic x-ray intensities of the Lyman series in carbon.

	det. 1[a]	det. 2	Mean	Ref. 4
Diamond				
(3-1)/(2-1)	0.258(10)	0.265(10)	0.261(8)	0.267(20)
(4-1)/(2-1)	0.125(5)	0.128(5)	0.126(4)	0.137(13)
(5-1)/(2-1)	0.032(2)	0.033(2)	0.033(2)	0.039(10)
(6-1)/(2-1)	0.006(1)	0.007(1)	0.007(1)	
Graphite				
(3-1)/(2-1)	0.284(10)	0.291(10)	0.288(8)	0.290(20)
(4-1)/(2-1)	0.141(5)	0.145(5)	0.143(4)	0.138(13)
(5-1)/(2-1)	0.037(2)	0.038(2)	0.037(2)	0.048(10)
(6-1)/(2-1)	0.008(1)	0.008(1)	0.008(1)	
Soot				
(3-1)/(2-1)	0.293(10)	0.301(10)	0.297(8)	
(4-1)/(2-1)	0.151(5)	0.153(5)	0.152(4)	
(5-1)/(2-1)	0.039(2)	0.042(2)	0.041(2)	
(6-1)/(2-1)	0.008(1)	0.009(1)	0.008(1)	

[a]det. 1 refers to the measurement with the 2-cm^3 Ge detector and det. 2 to the 13-cm^3 one.

mond allotropes of boron nitride is illustrated in Fig. 3, which includes data from all three detectors.

For all these relative intensities of the carbon- and the boron-nitride targets, the intensity contributions from carbon and nitrogen due to background have not been subtracted. In any case, these background lines are of low intensity and could at most lower the differences observed in Figs. 2 and 3.

The muonic carbon background lines are mainly due to muons stopped in the adhesive of the target holder and in the telescope counters. From the spectra taken with the boron-nitride target, the intensities of these muonic carbon background lines were estimated to be about 0.5% of the true carbon lines from muons trapped in the target material. This is considerably smaller than the uncertainty given in Table I on the individual muonic intensities.

Similarly, the nitrogen background coming mostly from muons stopped in the air was estimated from the spectra of muonic carbon in the diamond and

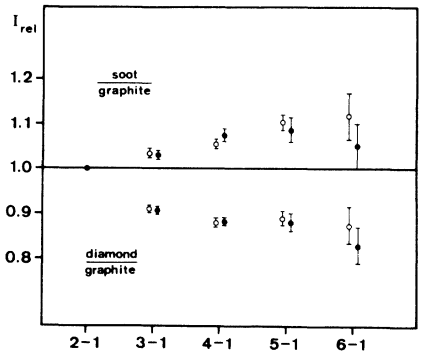

FIG. 2. Muonic Lyman-series intensities normalized to the respective (2-1) intensities in diamond and soot relative to graphite. I_{rel} means the $(n\text{-}1)/(2\text{-}1)$ intensity ratio in soot or diamond divided by the same ratio in graphite, with n running from 2 to 6. Solid points correspond to the measurement with the 2-cm^3 Ge(Li) detector, the open circles to that with the intrinsic 13-cm^3 Ge detector. Error bars correspond to the statistical error only.

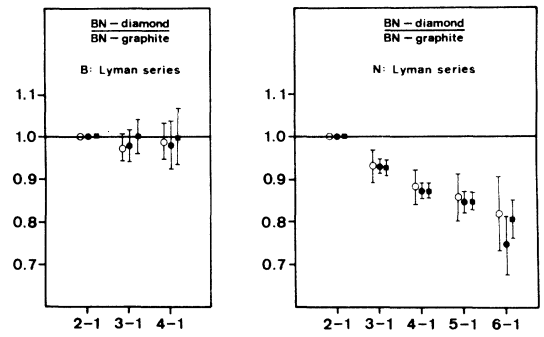

FIG. 3. Muonic Lyman-series intensities of boron and nitrogen normalized to the respective (2-1) intensities in the diamond allotrope of boron nitride relative to its graphite allotrope. Hollow circles correspond to the measurement with the 2-cm^3 Ge(Li) detector, the full points to that with the 13-cm^3 detector. and the squares to the 66-cm^3 Ge detector.

TABLE II. Relative muonic x-ray intensities of the Lyman series in boron nitride.

	det. 1[a]	det. 2	Mean	Ref. 4
Cubic				
B (3-1)/(2-1)	0.277(10)	0.275(10)	0.276(8)	0.312(20)
B (4-1)/(2-1)	0.110(5)	0.104(5)	0.107(4)	
B (5-1)/(2-1)	0.021(4)	0.020(4)	0.020(3)	
N (3-1)/(2-1)	0.262(7)	0.262(7)	0.262(5)	0.266(20)
N (4-1)/(2-1)	0.156(4)	0.153(4)	0.155(3)	0.160(13)
N (5-1)/(2-1)	0.053(3)	0.053(3)	0.053(2)	0.060(12)
N (6-1)/(2-1)	0.013(2)	0.013(2)	0.013(2)	0.026(15)
Hexagonal				
B (3-1)/(2-1)	0.285(10)	0.281(10)	0.283(8)	0.305(20)
B (4-1)/(2-1)	0.111(5)	0.107(5)	0.109(4)	0.168(12)
B (5-1)/(2-1)	0.021(4)	0.020(4)	0.021(3)	
N (3-1)/(2-1)	0.281(7)	0.282(7)	0.282(5)	0.278(20)
N (4-1)/(2-1)	0.177(4)	0.176(4)	0.177(3)	0.166(16)
N (5-1)/(2-1)	0.061(3)	0.063(3)	0.062(2)	0.057(12)
N (6-1)/(2-1)	0.016(2)	0.018(2)	0.017(2)	0.058(15)

[a]det. 1 refers to the measurement with the 2-cm^3 Ge detector and det. 2 to the 13-cm^3 one.

graphite forms. For the smaller detector this nitrogen background intensity was of the order of 0.6%, for the larger one about 1.6%. Again, these corrections are smaller than the errors given in Table I.

Every muon which is captured into a μ-atomic orbit of an element must undergo at least one transition to the 1s state. The sum of all the transition intensities of the Lyman series of an element is therefore a measure of the capture probability into that element. If a muon is captured into levels with principal quantum number $n < 18$ one obtains from cascade calculations[12] that the sum of the radiative transition intensities of the Lyman series is larger than 0.99 per muon. Hence, Auger transitions can be neglected as long as one deals with accuracies of the order of a few percent. Direct radiative transitions from molecular states to the 1s state, as some models[2,13] imply, have not been observed,[6,14] but would be included in our summing procedure. The sum of the radiative Lyman-series intensities is therefore directly proportional to the capture probability into the considered element.

Applying this method for the determination of the capture probability into boron relative to nitrogen in boron nitride, one obtains the ratios shown in Table III for the diamond and graphite allotropes. For comparison, the ratios obtained by Knight *et al.*[4] for the same allotropes are also given. Our earlier published ratio obtained for the graphitic modification[15] is not included in this table. In light of the consistency of our new results obtained independently with three detectors, we have to con-

TABLE III. Experimental atomic capture ratios of boron to nitrogen in boron nitride.[a]

	det. 1	det. 2	det. 3	Mean	Ref. 4
A(B/N) cubic	0.236(15)	0.231(12)	0.232(13)	0.233(11)	0.235(20)
A(B/N) hexagonal	0.280(15)	0.274(13)	0.272(15)	0.275(12)	0.258(20)
$\frac{A(B/N)\text{: hexagonal}}{A(B/N)\text{: cubic}}$	1.19(5)	1.19(5)	1.17(5)	1.18(3)	

[a]Values obtained by summing up the Lyman-series x-ray intensities measured with the 2-cm^3 Ge(Li) detector (det. 1), the intrinsic 13-cm^3 Ge detector (det. 2), and the high-purity 66-cm^3 Ge detector (det. 3) in the diamond (cubic) and the graphite (hexagonal) modification. For comparison, the results of the earlier measurement of Knight *et al.* (Ref. 4) are also given.

clude that the error given in Ref. 15 has been strongly underestimated, due to specific intensity calibration problems at low energies. However, the main point at that time was to confirm the result of Knight *et al.*,[4] i.e., a ratio which was by a factor of 3 smaller than what was predicted by the Z law.

We would like to stress here the importance of measuring the same transitions with more than one detector. First, it allows a check of the efficiency calibration. Second, it allows a better evaluation of the uncertainties in the determined intensities. Not only background lines may alter the true intensities but also the continuous background may easily be underestimated, especially when the peak to background ratio is unfavorable.

Comparing our ratios of Table III with those of Knight *et al.*[4] there is excellent agreement for the diamond structure and reasonably good agreement for the graphite modification. The relatively large uncertainties did not allow Knight *et al.*[4] to conclude definitely that the capture ratios were different in the two allotropes. Only the present measurements reveal that there is a clear difference in these ratios. This is particularly evident in the ratios of the capture ratios given in Table III. These ratios of ratios are actually to a large degree independent of the uncertainties in the efficiency calibration of the detectors, because about half of the intensity of the Lyman series is contained in the $2p$-$1s$ transition.

IV. DISCUSSION OF THE RESULTS

A. Carbon

1. Muonic cascade in diamond and graphite

The fact that the allotropy of carbon influences the muonic cascade intensity pattern is not a surprise. Indeed, it has already been shown in phosphorus and selenium[6] that differences in the solid-state structure may modify this intensity pattern. However, different allotropies do not have as a necessary consequence a measurable modification of the muonic intensity structure, e.g., no difference could be measured in the muonic Lyman-series intensities between black (metallic) and red (polymeric) phosphorus.[6]

The difference in the Lyman-series intensities between the diamond and graphite forms of carbon (Fig. 2) is a systematic one. Compared to the (2-1) intensity, the $(n-1)$ intensities are from 10–20 % higher in graphite than in diamond. Assuming that the muon cascade proceeds in the same manner for both allotropes, one deduces from the observed trend that the lower angular momentum states are initially populated more strongly in graphite than in diamond. Cascade calculations confirm this deduction.

Cascade calculations were performed in order to deduce from measured muonic x-ray intensities an angular momentum distribution for the captured muons[12,16] in a level of principal quantum number n. We assumed a modified statistical distribution

$$P(l)=N(2l+1)e^{\alpha l}$$

with α as an adjustable parameter. The normalization constant N is determined through the normalization condition

$$\sum_{l=0}^{n-1} P(l)=1 \ .$$

The advantage of this distribution is that the populations of all angular momentum states are positive. Assuming linear or parabolic distributions, the fitted populations may become negative.

The electron shells are strongly perturbed by the cascading muon. In light muonic atoms, the K-shell refilling rate is therefore considerably smaller than in neutral atoms.[16] The refilling of the electronic K shell, characterized by the refilling width Γ_K, was considered as a second adjustable parameter varying between zero for a fully ionized atom and a value of $\Gamma_K=0.0864$ eV for a neutral carbon atom.[17] The refilling width Γ_K was fitted only in muonic diamond. For graphite and soot, the diamond value was used as a fixed input parameter.

Because of the interatomic bond, the electrons of the L shell are not L electrons in the proper sense. However, the computer code[12] needs an input for L electrons in order to allow for Auger electron ejection and K shell refilling. Assuming that the atomic capture of a muon proceed through ejection of one of these electrons and that in the early stage of the muonic cascade further L electrons are ejected, we assumed 1.5 L electrons with binding energy of 4.7 eV present at the start of the cascade calculation at the level of principal quantum number n.

The choice of the level n in which the angular momentum distribution is determined through the fit to the experimental intensities is somewhat arbitrary. We have chosen the level $n=13$. The calculated distributions for diamond, graphite, and soot are illustrated in Fig. 4. These distributions indeed show a higher population of lower angular momentum states in graphite compared to diamond. In soot this tendency is enhanced. It is interesting to observe that the initial distribution obtained for diamond is the purely statistical distribution $P(l)\propto 2l+1$, the parameter α being very small $(\alpha=-0.0053)$.

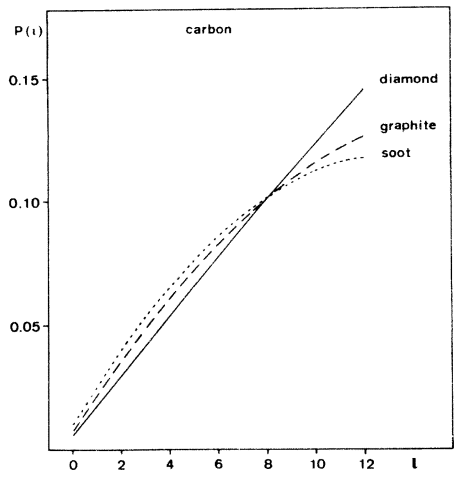

FIG. 4. Calculated muon angular momentum distributions in carbon in the level $n=13$ obtained through fits of the measured muonic Lyman-series intensities in diamond, graphite, and soot. Distribution was assumed to be a modified statistical one, $P(l)=N(2l+1)\exp(\alpha l)$. Diamond: $\alpha=-0.053$. Graphite: $\alpha=-0.0364$. Soot: $\alpha=-0.0544$.

Table IV contains the comparison of the experimental and calculated intensities for all three carbon targets together with the fitted parameters α and Γ_K. A purely statistical distribution for diamond would give the same χ^2.

Currently, no computer code for cascade calculations is really adapted to such light elements where one should take into account electrons in molecular orbits. Moreover, the assumed modified statistical distribution is not necessarily the best suited function to fit an initial distribution. Therefore, the calculated angular momentum distributions have to be taken with a certain circumspection.

2. *Muonic cascade in soot*

The measured difference in the muonic Lyman-series intensities between graphite and soot (Fig. 2) was unexpected, because the crystallite structures are actually the same, the only difference being in their size. It has already been pointed out that the inhomogeneity of the target material may influence the capture of the muon and that capture ratios may strongly depend on the grain size.[18,19] No predictions have been made concerning such a dependence for the pattern of the cascade intensities in an element. A recent measurement of Sn-Mg samples[20] revealed no systematic differences in the muonic Lyman-series intensity patterns depending on the inhomogeneity of the samples. Hence, the observed difference between graphite and soot is not expected to be due to the difference in the homogeneity of the target materials.

However, the specific surface area, determined by the mean sizes of the crystallites is about 10^3 times larger in soot than in graphite. The surface atoms have a spatial valence electron distribution which is slightly different from those inside the crystallites. However, too few carbon atoms are at the surface of the soot crystallites to justify the observed intensity differences in terms of electron density distributions.

Surfaces generally contain impurity elements. In the present case of carbon, these elements are mainly hydrogen and oxygen. In graphite, these foreign atoms at the surface are negligible compared to the total number of carbon atoms. In the soot, however,

TABLE IV. Calculated intensities with modified statistical $[P(l)\propto(2l+1)e^{\alpha l}]$ angular momentum distributions in $n=13$ obtained from the fit of the experimental muonic Lyman series in the three carbon targets. Γ_k is the K-electron refilling width.

	Diamond		Graphite		Soot	
C	Expt.	Calc.	Expt.	Calc.	Expt.	Calc.
2-1	0.701(12)	0.699	0.677(12)	0.676	0.667(12)	0.662
3-1	0.183(4)	0.184	0.195(4)	0.194	0.198(4)	0.200
4-1	0.088(3)	0.087	0.097(3)	0.096	0.101(3)	0.101
5-1	0.0229(8)	0.0217	0.0250(8)	0.0245	0.0272(8)	0.0263
6-1	0.0046(3)	0.0049	0.0053(3)	0.0058	0.0057(3)	0.063
χ^2/DF	1.2/3		3.3/3		5.7/3	
α	−0.0053		−0.0364		−0.0544	
Γ_k (eV)	0.045		0.045		0.045	

the hydrogen impurity atoms represent about 2.4%, and the oxygen impurity atoms about 3.6% of the total number of carbon atoms since the specific surface area as determined from the average sizes of the crystallites is about 1000 times larger in soot than in graphite. The analysis of our muonic data shows that the oxygen and nitrogen background is the same (within 2%) for the diamond and graphite targets. In soot, the nitrogen background—serving as a reference—is still very low and only slightly, i.e., by about 30%, higher than in the other two allotropes, whereas the oxygen background is increased by a factor of about three. This corresponds to about 3% oxygen in the soot target, in agreement with the chemical analysis. In order to extract from the muonic data the exact amount of oxygen in the target,[21] one would have to know details of the C—O bond.

From our intensity measurements, the amount of hydrogen in the soot target cannot be extracted because the hydrogen Lyman series cannot be measured with our experimental setup. It is well known, however, that bound hydrogen drastically changes the muonic Lyman-series intensity structure of the bond partners.[4,22,23] In particular, the intensities of the higher members of the Lyman series are enhanced by the bound hydrogen. This enhancement is to a great extent due to the transfer of the muon from the neutral μp system to the heavier element. Indeed, transferred muons preferentially populate low l states, as has been shown by calculation[24] and by various experiments with gases and solids.[25–28] We can therefore conclude that the 2.4% hydrogen in the soot target may well be responsible, by means of muon transfer, for the observed difference between graphite and soot (Fig. 2).

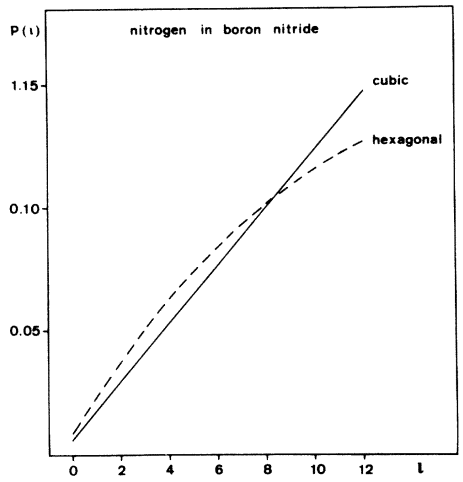

FIG. 5. Calculated muon angular momentum distributions in nitrogen in the level $n=13$ obtained through fits of the measured muonic Lyman-series intensities in cubic and hexagonal boron nitride. Parameters of the modified statistical distribution: Cubic, $\alpha=-0.0022$; hexagonal, $\alpha=-0.0399$.

B. Boron nitride

1. Muonic cascade in nitrogen

The distribution over angular momentum states of the muons captured in nitrogen of both allotropes of boron nitride have been determined in the same way as for the carbon targets. The same reservations have therefore to be considered for the fitted distributions.

Apart from the conventional inputs in the cascade program[12] we assumed for nitrogen that three of five L electrons with binding energies of 6.4 eV were present at the beginning of the cascade calculation at $n=13$. The refilling width of the electronic K shell was fitted in the diamond structure and gave a minimum χ^2 for $\Gamma_K=0.04$ eV. The calculated angular momentum distributions in the level $n=13$ for nitrogen in both boron nitride allotropes are illustrated in Fig. 5. The comparison of the measured and the calculated intensities is given in Table V.

One observes that, like in carbon, the distribution for nitrogen in the diamond structure of boron nitride is compatible with the purely statistical distribution. In the graphitic structure the population of lower angular momentum states is enhanced similarly to what was observed in carbon.

These similarities of the muon distributions in carbon and nitrogen for the cubic and hexagonal structures are striking. They are correlated to similarities in the electronic structures. No differences in the intensities of the Lyman series in boron have been observed in the two modifications, at least up to the measured (4-1) transition. Currently, we have no explanation for such a different behavior compared to nitrogen.

2. Boron-to-nitrogen capture ratios

The fact that the boron-to-nitrogen capture ratios are different for the two allotropes of boron nitride shows how strongly the capture rate is influenced by the electronic structure of the bond between elements. This difference (Table III) of 18 ± 3% can only be due to a difference in the spatial electron density distributions between the cubic and hexago-

TABLE V. Calculated intensities with modified statistical $[P(l) \propto (2l+1)e^{\alpha l}]$ angular momentum distributions in $n=13$ obtained from the fit of the experimental muonic Lyman series intensities in nitrogen of boron nitride in diamond and graphitic structure. Γ_k is the K-electron refilling width.

	Diamond		Graphitic	
N of BN	Expt.	Calc.	Expt.	Calc.
2-1	0.674(10)	0.670	0.651(10)	0.649
3-1	0.177(4)	0.175	0.183(4)	0.179
4-1	0.104(3)	0.105	0.115(3)	0.115
5-1	0.0357(12)	0.0345	0.0405(12)	0.0396
6-1	0.0088(5)	0.091	0.0110(5)	0.0109
χ^2/DF	2.0/3		2.2/3	
α	−0.0022		−0.0399	
Γ_k (eV)	0.04		0.04	

nal structure of boron nitride.

In our model[2] developed to predict capture ratios, we assumed that the spatial distribution of the valence electron density influences the capture probabilities. In order to describe this distribution, we need a numerical quantity which is known or at least defined between all partners of a compound. In an explicit version of the model, we used the ionicity σ defined by Pauling[29] as the parameter related to this spatial valence electron distribution realizing that it can only be a rough approximation. Assuming the validity of our model, one can extract this parameter from the measured capture ratios. This formula used for the capture ratio into the two elements of a binary compound of elements with charge numbers Z_1 and Z_2 is

$$A\left[\frac{Z_1}{Z_2}\right]=\frac{\nu(1-\sigma)Z_1^2/X+n_1}{\nu(1+\sigma)Z_2^2/X+n_2},$$

where ν is the number of electrons involved in the bond, n_i the number of remaining core electrons of element Z_i with binding energies less than E_0, and

$$X=(1-\sigma)Z_1^2+(1+\sigma)Z_2^2,$$

a normalization constant. Z_2 is the charge number of the element with greater electronegativity.

In the case of boron nitride $Z_1(\mathrm{B})=5$, $Z_2(\mathrm{N})=7$, we assumed that both elements have valence three. Thus, $\nu=6$ and, with $E_0=60$ eV, $n_1=0$ and $n_2=2$. The capture ratio as a function of the parameter σ is drawn in Fig. 6 and compared to the experimental capture ratios. In order to achieve agreement between the model predictions and the experimental values, this parameter should be about $\sigma=0.10$ for the graphitic structure and $\sigma=0.20$ for the diamond structure of boron nitride.

On the other hand, we can use the numerical value of the ionicity as defined by Pauling through a formula containing the electronegativities of the elements. For the B—N bond, this value is $\sigma=0.22$, independent of the structure of boron nitride. Using this value as an input, the model prediction for the boron-to-nitrogen capture ratio is then $A(\mathrm{B/N})=0.23$, in agreement with our experimental ratio in the cubic structure.

V. CONCLUSIONS

The formation of exotic atoms is still insufficiently understood despite numerous experimental studies

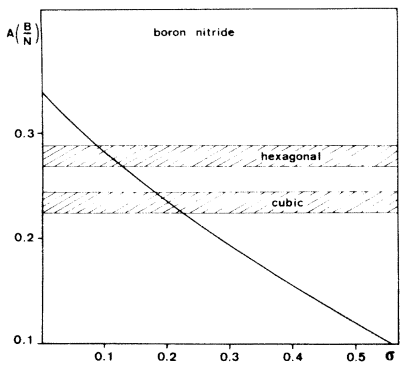

FIG. 6. Comparison of the measured boron-to-nitrogen capture ratios obtained in the cubic and hexagonal structures of boron nitride with the model predictions as a function of the ionicity σ of the B—N bond.

and theoretical endeavors. The present experiment, like our earlier ones,[3,6,15,30] should help to clarify how sensitive the muon capture mechanism is to the structure of the valence electron cloud.

Our experimental results confirm that the lighter the atom the greater the influence of the valence electron cloud on the capture mechanism.[3] The comparison of the muonic x-ray intensity structures in carbon and nitrogen and of the fitted distributions of the captured muons over angular momentum states shows that the muon capture mechanism is sensitive to the symmetries of the crystalline structures. It is remarkable that for the cubic structures the fitted angular momentum distributions are statistical both for carbon and nitrogen, and that the deviations from the statistical distribution in the hexagonal structures are similar for both elements.

We have found a clear difference in the boron-to-nitrogen capture ratios between the cubic and hexagonal boron nitride. The difference is of the order of 20% and therefore shows clearly that the capture through the valence electrons is dominant in such light atoms.

Our model[2] reproduces the measured boron-to-nitrogen capture ratios because it takes the chemical bond into account. It assumes that the $1s$ electrons of boron and nitrogen do not participate directly in the atomic capture of muons and that only their L electrons are involved. In its present version the model contains only a simiplified picture of the chemical bond because it assumes that the $2s$ electrons of nitrogen do not participate in the bonding so that only six electrons are involved in the B—N bonds. Yet, the difference in the boron-to-nitrogen capture ratios can be reproduced assuming a redistribution of the valence electrons. The needed values of the parameter σ are about 0.10 for the hexagonal boron nitride and about 0.20 for its cubic structure. Whether this parameter σ can be interpreted as the ionicity of the bond or whether is is related to the valence electron distribution in another way remains to be seen.

ACKNOWLEDGMENTS

The authors wish to thank Dr. C. Daul for many fruitful discussions and Dr. P. Vogel for helpful comments.

[1]H. Schneuwly, in *Proceedings of the First Course of the International School of Physics of Exotic Atoms, Erice 24—30 April 1977,* edited by G. Fiorentini and G. Torelli (Servizio Documentazione dei Laboratori Nazionali di Frascati, Frascati, 1977), p. 255.

[2]H. Schneuwly, V. I. Pokrovsky, and L. I. Ponomarev, Nucl. Phys. A312, 419 (1978).

[3]H. Schneuwly, T. Dubler, K. Kaeser, B. Robert-Tissot, L. A. Schaller, and L. Schellenberg, Phys. Lett. 66A, 188 (1978).

[4]J. D. Knight, C. J. Orth, M. E. Schillaci, R. A. Naumann, H. Daniel, K. Springer, and H. B. Knowles, Phys. Rev. A 13, 43 (1976).

[5]T. Dubler, K. Kaeser, B. Robert-Tissot, L. A. Schaller, L. Schellenberg, and H. Schneuwly, Nucl. Phys. A294, 397 (1978).

[6]K. Kaeser, T. Dubler, B. Robert-Tissot, L. A. Schaller, L. Schellenberg, and H. Schneuwly, Helv. Phys. Acta 52, 238 (1979).

[7]L. A. Schaller, L. Schellenberg, A. Rüetschi, and H. Schneuwly, Nucl. Phys. A343, 333 (1980).

[8]R. J. Gehrke, R. G. Helmer, and R. C. Greenwood, Nucl. Instrum. Methods 147, 405 (1977).

[9]*Table of Isotopes,* 7th ed., edited by C. M. Lederer and V. S. Shirley (Wiley, New York, 1978).

[10]M. Boschung, Masters thesis, Institut de Physique de l'Université de Fribourg, 1980 (unpublished).

[11]E. Storm and H. I. Israel, 1980 At. Data Nucl. Data Tables 7, 565 (1970).

[12]V. R. Akylas and P. Vogel, Comput. Phys. Commun. 15, 291 (1978).

[13]S. S. Gershtein, V. I. Petrukhin, L. I. Ponomarev, and Yu. D. Prokoshkin, Usp. Fiz. Nauk 97, 3 (1969) [Sov. Phys.—Usp. 12, 1 (1969)].

[14]K. Andert, R. Engfer, H. Haupt, V. S. Evseev, H. G. Ortlepp, V. S. Roganov, B. M. Sabirov, and H. Schneuwly, *High Energy Physics and Nuclear Structure—1975,* proceedings of the Sixth International Conference, Santa Fé and Los Alamos, edited by D. E. Nagle *et al.* (AIP, New York, 1975), p. 155.

[15]T. Dubler, K. Kaeser, B. Robert-Tissot, L. A. Schaller, L. Schellenberg, and H. Schneuwly, Phys. Lett. 57A, 325 (1976).

[16]P. Vogel, Phys. Rev. A 22, 1600 (1980).

[17]E. J. McGuire, Phys. Rev. A 2, 273 (1970).

[18]H. Daniel, Nucl. Instrum. Methods 150, 609 (1978).

[19]H. Daniel and M. Leon, Nucl. Instrum. Methods 158, 232 (1979).

[20]R. Bergmann, H. Daniel, T. von Egidy, F. J. Hartmann, and W. Wilhelm, Z. Phys. A 299, 297 (1981).

[21]J. D. Knight, C. J. Orth, M. E. Schillaci, R. A. Naumann, F. J. Hartmann, J. J. Reidy, and H. Schneuwly, Phys. Lett. 79A, 377 (1980).

[22]H. Daniel, H. Koch, G. Poelz, H. Schmitt, L. Tauscher, G. Backenstoss, and S. Charalambus, Phys. Lett. 26B, 281 (1968).

[23]C. R. Cox, G. W. Dodson, M. Eckhause, R. D. Hart, J. R. Kane, A. M. Rushton, R. T. Siegel, R. E. Welsh, A.

L. Carter, M. S. Dixit, E. P. Hincks, C. K. Hargrove, and H. Mes, Can. J. Phys. 57, 1746 (1979).

[24]G. Holzwarth and H. J. Pfeiffer, Z. Phys. A 272, 311 (1975).

[25]Yu. G. Budyashov, P. F. Ermolov, Y. G. Zinov, A. D. Konin, and A. I. Mukhin, Yad. Fiz. 5, 830 (1967) [Sov. J. Nucl. Phys. 5, 426 (1967)].

[26]H. Daniel, H. J. Pfeiffer, and K. Springer, Phys. Lett. 44A, 447 (1973).

[27]A. Bertin, F. Ferrari, I. Massa, M. Piccinini, G. Vannini, and A. Vitale, Phys. Lett. 68A, 201 (1978).

[28]E. Iacopini, G. Carboni, G. Torelli, and V. Trobbiani, Nuovo Cimento A 67, 201 (1982).

[29]L. Pauling, *The Nature of the Chemical Bond and the Structure of Molecules and Crystals* (Cornell University Press, Ithaca 1960).

[30]K. Kaeser, B. Robert-Tissot, L. A. Schaller, L. Schellenberg, and H. Schneuwly, Helv. Phys. Acta 52, 304 (1979).